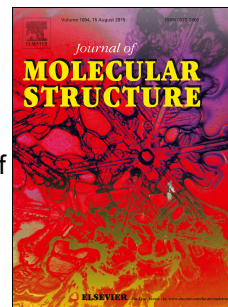


Accepted Manuscript

Role of co-ligand and solvent on properties of V(IV) oxido complexes with ONO Schiff bases

Janusz Szklarzewicz, Anna Jurowska, Maciej Hodorowicz, Ryszard Gryboś, Dariusz Matoga



PII: S0022-2860(18)31474-1

DOI: <https://doi.org/10.1016/j.molstruc.2018.12.047>

Reference: MOLSTR 25984

To appear in: *Journal of Molecular Structure*

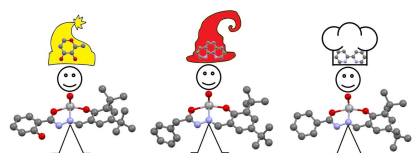
Received Date: 29 August 2018

Revised Date: 21 November 2018

Accepted Date: 11 December 2018

Please cite this article as: J. Szklarzewicz, A. Jurowska, M. Hodorowicz, R. Gryboś, D. Matoga, Role of co-ligand and solvent on properties of V(IV) oxido complexes with ONO Schiff bases, *Journal of Molecular Structure* (2019), doi: <https://doi.org/10.1016/j.molstruc.2018.12.047>.

This is a PDF file of an unedited manuscript that has been accepted for publication. As a service to our customers we are providing this early version of the manuscript. The manuscript will undergo copyediting, typesetting, and review of the resulting proof before it is published in its final form. Please note that during the production process errors may be discovered which could affect the content, and all legal disclaimers that apply to the journal pertain.



Role of co-ligand and solvent on properties of V(IV) oxido complexes with ONO Schiff bases

Janusz Szklarzewicz^{a*}, Anna Jurowska^a, Maciej Hodorowicz^a, Ryszard Gryboś^a and Dariusz Matoga^a

^a Faculty of Chemistry, Jagiellonian University, Gronostajowa 2, 30-387 Kraków, Poland

Abstract

Four complexes of V(IV/V) of octahedral geometry, with tridentate ONO Schiff base ligand, oxido and bidentate (maltol, 1,10-phenantroline or 2,2'-bipyridine) co-ligands are described. The Schiff bases were formed from 3,5-di-tert-butyl-2-hydroxybenzaldehyde and hydrazides (benzhydrazide, 2-hydroxybenzhydrazide and phenylacetic hydrazide). The X-ray single-crystal structures of all complexes revealed that they are a mixture of 1:1 isomers with the different position of 5- and 6-membered ring of ONO ligand *versus* V=O, excluding **1**. The position of the V=O band in IR spectra was found to be dependent on the V=O and *trans* located donor atom bond distances. Two complexes, **3** and **3a**, were isolated as unsolvated and solvated ones, the coordination of solvent molecule drastically changed the structure parameters. The cyclic voltammetry measurements show irreversible processes for vanadium redox system and reversible ones for co-ligands. The stability of complexes in solution is discussed.

Keywords: vanadium, complex, co-ligand, Schiff base, structure.

Introduction

The chemistry of vanadium is widely investigated as the biological role of vanadium compounds including anticancer, insulin-mimetic, anti-inflammatory and antibacterial belong to the most relevant ones [1-9]. One of the last founding is that vanadium complexes can significantly reduce the resistance to oncolytic immunotherapy [10-13]. The question is in which form vanadium is incorporated to biological systems. It was found, that in case of

mono and bidentate ligands and V(IV), simple VO^{2+} ions are active. Our last investigations show however, that with more polydentate ligands complexes are much more stable and the type of ligand is important and affects biological activity [14]. This may suggest, that unchanged complex is active, thus the ligand type may modify the vanadium activity. The main problem with polydentate ligands is that not all types of ligands can fill the coordination sphere of vanadium, thus additional co-ligands are observed in structure. In case of solvent molecules, which can be easily exchanged, the complex stability seems to be low [15,16]. As vanadium(IV) is mostly octahedral (but also pentadentate ligand complexes are observed [17,18]) this reduces the ligands type to pentadentate, tetradentate (but only for penta-coordinated vanadium) or tridentate. For tetradentate ligand complexes, we have found that the complex stability is high [14], even possessing distorted square pyramidal geometry. For tridentate ligands, presented in this paper, bidentate co-ligands are necessary to increase the complex stability in solution. It was found also, that 1,10-phenantroline, used as co-ligand, stabilise the oxidation state of vanadium, otherwise complexes are very sensitive on oxygen and are oxidized to V(V) [16].

We have lastly studied the complexes with Schiff bases composed from 5-bromosalicylaldehyde and benzhydrazide or 4-tertbutylbenzhydrazide and we have found that they are active in inhibition of human recombinant PTP1B, one of them was found to be twice as active as suramin [16] and we presented the selected data of their stability in neutral and acidic ($\text{pH} = 2.0$) conditions. In present paper we discuss the role of type of co-ligands on vanadium(IV/V) complexes properties. We used Schiff bases formed from 3,5-di-tert-butyl-2-hydroxybenzaldehyde and hydrazides - 2-hydroxybenzhydrazide (L_1) phenylacetic hydrazide (L_2) and benzhydrazide (L_3), to have a very similar type of ONO ligand. As co-ligands, we used maltol - typical ligand in insulin mimetic properties, mostly known in its application as bismaltolatoovanadium complex (BMOV) [19], 1,10-phenantroline (phen) or 2,2'-bipyridine(bpy). Two first ligands are rigid, while bpy molecule, as more flexible, could be easier substituted, thus the stability of investigated complexes in solution is discussed.

Experimental

Materials and methods

[VO(acac)₂], [VOSO₄] monohydrate, 1,10-phenanthroline (phen), maltol (mal denote maltolato ligand), 2,2'-bipyridine (bpy), 3,5-di-tert-butyl-2-hydroxybenzaldehyde, 2-hydroxybenzhydrazide, phenylacetic hydrazide and benzhydrazide were of analytical grade (Aldrich) and were used as supplied. Ethanol (98%) of pharmaceutical grade was from Polmos (Poland) and used as supplied. All other solvents were of analytical grade and were used as supplied. BaSO₄ were of spectroscopic grade (Japan). [Bu₄N]PF₆ was synthesized from Bu₄NBr and KPF₆ by a standard method and recrystallized from acetone [20]. Microanalysis of carbon, hydrogen and nitrogen were performed using Elementar Vario MICRO Cube elemental analyzer. IR spectra were recorded on a Bruker EQUINOX 55 FT-IR spectrophotometer in KBr pellets. The electronic absorption spectra were recorded on Shimadzu UV-3600 UV-VIS-NIR spectrophotometer equipped with a CPS-240 temperature controller. Diffuse reflectance spectra were measured in BaSO₄ pellets with BaSO₄ as a reference on Shimadzu 2101PC equipped with an ISR-260 integrating sphere attachment. The magnetic susceptibility measurements were performed on a SHERWOOD SCIENTIFIC magnetic susceptibility balance. Cyclic voltammetry measurements were carried out in DMSO with [Bu₄N]PF₆ (0.1 M) as the supporting electrolyte, using Pt working and counter and Ag/AgCl as reference electrodes on an AUTOLAB/PGSTAT 128 N Potentiostat/Galvanostat. $E_{1/2}$ values were calculated from the average anodic and cathodic peak potentials, $E_{1/2} = 0.5(E_a + E_c)$. The redox potentials were calibrated *versus* ferrocene (0.440 V *versus* SHE), which was used as an internal potential standard for measurements in organic solvents to avoid the influence of a liquid junction potential; the final values are reported versus the standard hydrogen electrode (SHE). DTG measurements were performed on a TGA/SDTA 851e Mettler Toledo Microthermogravimeter under argon atmosphere in the 25-700 °C range with scan speed 10 °C/min.

Crystallographic data collection and structure refinement

Diffraction intensity data for single crystal of four new compounds (**1**, **2**, **3** and **3a**) were collected at 293(2) K on a KappaCCD (Nonius) diffractometer with graphite-monochromated MoK α radiation ($\lambda = 0.71073$ Å). Cell refinement and data reduction were performed using firmware [21,22]. Positions of all of non-hydrogen atoms were determined by direct methods using SIR-97 [23]. All non-hydrogen atoms were refined anisotropically using weighted full-matrix least-squares on F^2 . Refinement and further calculations were carried out using SHELXL 2014/7 [24]. All hydrogen atoms joined to carbon atoms were positioned with an idealized geometries and refined using a riding

model with $U_{\text{iso}}(\text{H})$ fixed at $1.5 U_{\text{eq}}$ of C for methyl groups and $1.2 U_{\text{eq}}$ of C for other groups. CCDC 181172, 1844928, 1850268 and 1848816 of **1**, **2**, **3** and **3a** respectively contain the supplementary crystallographic data. These data can be obtained free of charge from The Cambridge Crystallographic Data Centre via www.ccdc.cam.ac.uk/data_request/cif.

Synthesis of $[\text{VO}(\text{L}_1)(\text{mal})]$ (**1**)

The 3,5-di-tert-butyl-2-hydroxybenzaldehyde (0.355 g, 1.5 mmol) and the 2-hydroxybenzhydrazide (0.228 g, 1.5 mmol) were dissolved in 30 ml of EtOH under Ar. The mixture was refluxed for 20 minutes under argon and $\text{VO}(\text{SO}_4)_2$ (0.333 g, 1.5 mmol) was added. The mixture was refluxed for next 30 minutes. The solution becomes dark green-brown. During reflux black crystals started to precipitate. At this stage, maltol (0.190 g, 1.5 mmol) was added and mixture was refluxed 15 minutes. The solution becomes transparent without deposition. The solvent was then evaporated to half its starting volume and the mixture was cooled under argon. The initially formed black crystals were removed by filtration, the filtrate was left on air and after ca. 3 hours the dark-red crystals were filtered off, washed with EtOH and dried in air. Yield: 0.185 g, 22 %. MW 559.51. Anal. Calcd. for $\text{C}_{28}\text{H}_{32}\text{N}_2\text{O}_7\text{V}$: C, 60.11; H, 5.76; N, 5.01 %. Found: C, 59.82; H, 5.64; N, 4.78 %. The complex is diamagnetic.

Synthesis of $[\text{VO}(\text{L}_2)(\text{phen})]$ (**2**)

The 3,5-di-tert-butyl-2-hydroxybenzaldehyde (0.254 g, 1.5 mmol), phenylacetic hydrazide (0.227 g, 1.5 mmol) and 50 ml of EtOH were refluxed for 15 minutes under Ar. To the solution $[\text{VO}(\text{acac})_2]$ (0.398 g, 1.5 mmol) was added and the mixture was refluxed for 40 minutes. Then 1,10-phenantroline (0.271 g, 1.5 mmol) was added and the mixture was refluxed for next 15 minutes. The transparent solution was evaporated to ca. 40 ml and was left for next day. The very fine crystalline product was filtered off, washed with EtOH and dried in air. Yield 0.189 g, 29%. MW = 611.62. Anal. Calcd. for $\text{C}_{35}\text{H}_{36}\text{N}_4\text{O}_3\text{V}$: C, 68.73; H, 5.93; N, 9.16 %. Found: C, 67.34; H, 5.62; N, 9.42 %. The complex is paramagnetic, $\mu = 1.58 \mu_{\text{B}}$.

Synthesis of $[\text{VO}(\text{L}_3)(\text{bpy})] \cdot \text{MeOH}$ (**3**)

The 3,5-di-tert-butyl-2-hydroxybenzaldehyde (0.7060 g, 3.0 mmol), benzhydrazide (0.420 g, 3.0 mmol) and 50 ml of MeOH were refluxed for 8 minutes. To the solution 1.38 ml of Et₃N, VOSO₄aq (0.667 g, 3.0 mmol) and 10 ml of MeOH were added and refluxed for 20 minutes. During this period solution becomes dark red. Then 2,2'-bipyridine (0.472 g, 3.0 mmol) in 10 ml of MeOH was added and heated for 3 minutes and cooled. Complex was filtered off, washed with MeOH and dried in air. Yield 1.086 g, 60%. MW = 605.62. Anal. Calcd. for C₃₃H₃₈N₄O₄V: C, 65.45; H, 6.32; N, 9.25 %. Found: C, 65.76; H, 6.37; N, 9.30 %. The complex is paramagnetic, $\mu = 1.22 \mu_B$.

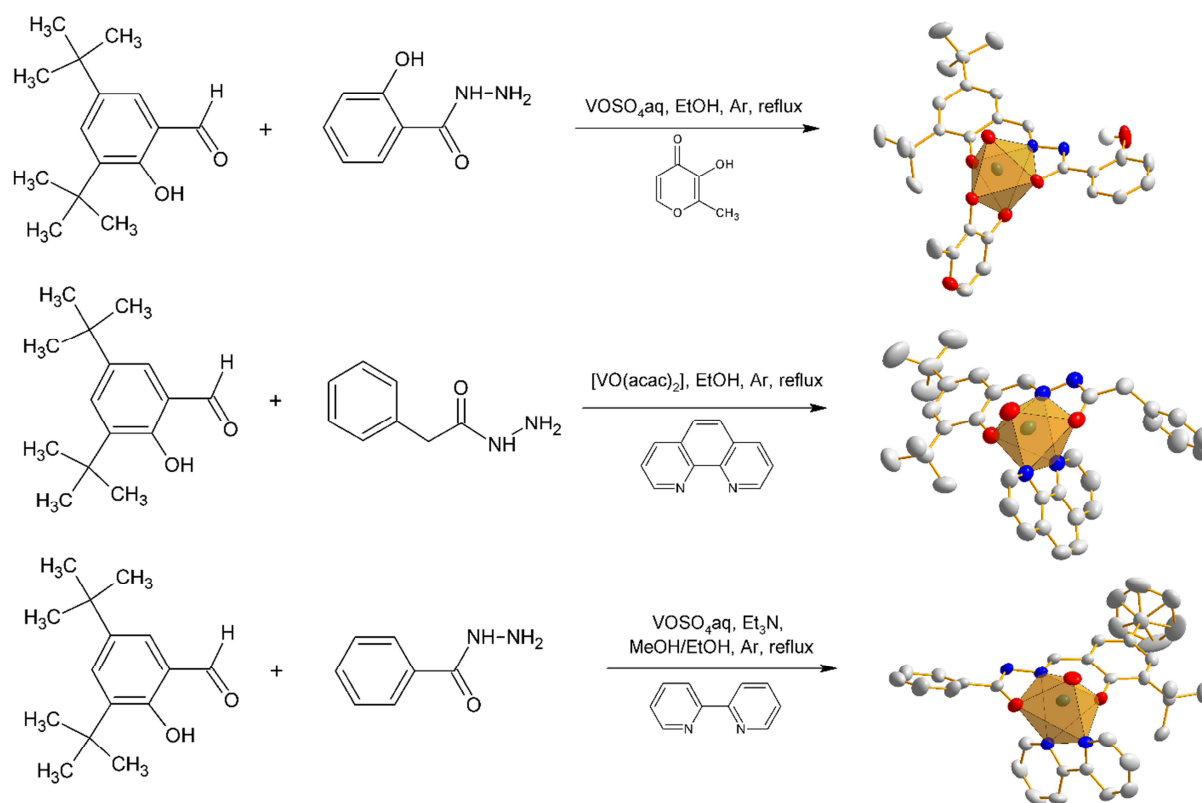
Synthesis of [VO(L₃)(bpy)]·EtOH (3a)

The 3,5-di-tert-butyl-2-hydroxybenzaldehyde (0.705 g, 3.0 mmol), benzhydrazide (0.408 g, 3.0 mmol) and 60 ml of EtOH were refluxed for 6 minutes. To the solution 1.38 ml of Et₃N was added and mixture was refluxed for additional 5 minutes. Then VOSO₄aq (0.666 g, 3.0 mmol) was added and refluxed for 20 minutes. During this period solution becomes dark red. The solution was filtered under Argon and 2,2'-bipyridine (0.468 g, 3.0 mmol) was added and heated for next 5 minutes. The crystals formed were filtered off under Ar, washed with cold EtOH and dried in air. Yield 0.804 g, 43 %. The filtrate was evaporated under Ar to one third of the initial volume and additional 0.286 g of complex was collected by filtration. Total yield: 1.090 g, 59 %. MW = 619.65. Anal. Calcd. for C₃₄H₄₀N₄O₄V: C, 65.90; H, 6.51; N, 9.04 %. Found: C, 65.44; H, 6.42; N, 8.91 %. The complex is paramagnetic, $\mu = 1.58 \mu_B$.

Results and discussion

General remarks to the synthesis

The reaction of *in situ* formed Schiff base ligands with vanadium salts results in its coordination to metal center (see Scheme 1.). The obtained solutions do not crystallize easily, and to get stable complexes, bidentate co-ligands were added. As we utilized 3 different hydrazides and 3 different co-ligands, there is 9 possible combinations. But only in case **1-3a** we got crystals suitable for X-ray measurements. In other cases, complexes (especially with maltol) were unstable or did not crystallize or oil products were formed. Complexes **1-3a** are stable in a solid state and were kept in closed vials, 8 years after preparation no changes were observed.



Scheme 1. Synthesis scheme for **1-3** complexes.

Description of the structures of **1-3a**

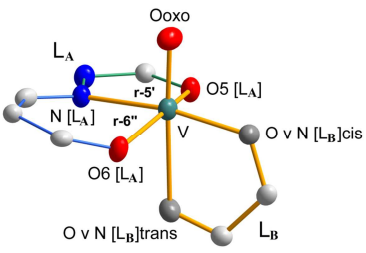
The complexes **1-3a** are neutral, in two cases solvent molecules were found by elemental analysis and IR spectra (described later in this paper). The solvent molecules could not be located precisely in the X-ray crystal structure determination and were omitted in final refinement. For complex **3**, solvent disorder caused low quality of the final refinement, thus the checkcif could not be deposited (only cif file was deposited). Nevertheless, the structure was resolved and is discussed here. The asymmetric parts of the units cells of the complexes **1-3a** with adopted atomic numbering scheme are shown in Figs 1 and 2. Single crystals of the compounds were obtained directly as described in the syntheses. The complex **1** crystallizes in the orthorhombic (**1** and **3a**) or monoclinic (**2** and **3**) space groups $P2_12_12_1$ (**1**), $P2_1/c$ (**2**), $P2_1/c$ (**3**), $Pbca$ (**3a**) with the asymmetric cell unit containing one molecule of $[VOL_A L_B]$ complex, where L_A denote ligand L_1 , L_2 or L_3 , L_B denote maltol, phen or bpy as indicated in Table 2. The crystallographic data and detailed information on the structure solution and refinement are given in Table 1. Selected

bond distances and bond angles are listed in Table 2. As depicted in Figs 1 and 2 the oxovanadium cation (VO^{2+}) is coordinated to the tridentate hydrazone ligand, through the phenolate oxygen (O), azomethine nitrogen (N) and enolate oxygen (O), and a bidentate L_B ligand (OO or NN type for maltol or bpy and phen respectively). Thus in all complexes the vanadium has distorted octahedral geometry.

Table 1 Crystal data and structure refinement parameters for **1-3a**.

	1	2	3	3a
Empirical formula	C ₂₈ H ₃₁ N ₂ O ₇ V	C ₃₅ H ₃₆ N ₄ O ₃ V	C ₃₂ H ₃₄ N ₄ O ₃ V	C ₃₂ H ₃₄ N ₄ O ₃ V
Formula weight	558.49	611.62	573.57	573.57
Crystal size (mm)	0.320 x 0.120 x 0.040	0.200 x 0.200 x 0.200	0.280 x 0.260 x 0.050	0.190 x 0.100 x 0.040
Crystal system	Orthorhombic	Monoclinic	Monoclinic	Orthorhombic
Space group	P 2 ₁ 2 ₁ 2 ₁	P 2 ₁ /c	P 2 ₁ /c	P bca
a (Å)	8.894(5)	14.9200(3)	25.018(2)	19.757(5)
b (Å)	9.535(5)	16.2740(3)	9.8290(17)	11.748(5)
c (Å)	32.554(5)	19.9320(3)	12.378(5)	28.831(5)
α (°)	90.000(5)	90	90	90
β (°)	90.000(5)	130.2810(10)	94.934(13)	90
γ (°)	90.000(5)	90	90	90
h	-10 ≤ h ≤ 10	-19 ≤ h ≤ 18	-24 ≤ h ≤ 25	-15 ≤ h ≤ 26
k	-9 ≤ k ≤ 11	-20 ≤ k ≤ 21	-10 ≤ k ≤ 10	-7 ≤ k ≤ 15
l	-38 ≤ l ≤ 23	-25 ≤ l ≤ 25	-11 ≤ l ≤ 12	-25 ≤ l ≤ 38
V (Å ³)	2761(2)	3692.08(12)	3032.5(12)	6692(4)
Z	4	4	4	8
T (K)	293(2)	293(2)	293(2)	293(2)
Wavelength [Å]	0.71069	0.71073	0.71073	0.71073
D _x (Mg/m ³)	1.344	1.100	1.256	1.139
Absorption coefficient (mm ⁻¹)	0.407	0.303	0.365	0.331
Theta range for data collection (°)	3.132 to 24.987	2.839 to 27.498	3.038 to 21.468	3.429 to 28.582
Reflections collected	6160	30312	6904	21544
Independent reflections	4454 [R(int) = 0.0258]	8405 [R(int) = 0.0351]	3126 [R(int) = 0.0800]	7704 [R(int) = 0.0953]
Completeness to theta	99.1 % (24.987°)	99.0 % (25.242°)	90.1 % (21.468°)	99.6 % (25.242°)
Absorption correction	Semi-empirical from equivalents	None	Semi-empirical from equivalents	none
Refinement method	Full-matrix least-squares on F ²	Full-matrix least-squares on F ²	Full-matrix least-squares on F ²	Full-matrix least-squares on F ²
Data / restraints / parameters	4454 / 1 / 355	8405 / 0 / 394	3126 / 0 / 392	7704 / 0 / 356
Goodness-of-fit on F ²	0.967	1.046	1.084	0.825
Final R indices [I > 2σ(I)]	R1 = 0.0571, wR2 = 0.1389	R1 = 0.0754, wR2 = 0.2206	R1 = 0.0739, wR2 = 0.1360	R1 = 0.0719, wR2 = 0.1766
R indices (all data)	R1 = 0.0838, wR2 = 0.1473	R1 = 0.1008, wR2 = 0.2548	R1 = 0.1407, wR2 = 0.1569	R1 = 0.1979, wR2 = 0.2097
Largest diff. peak and hole (e.Å ⁻³)	0.674 and -0.265	1.320 and -0.280	0.224 and -0.210	0.692 and -0.455

Table 2 Selected bond distances [\AA] in complexes **1-3a** with the figure showing general coordination scheme around vanadium center.



	1	2	3	3a
V=O	1.583(5)	1.593(2)	1.598(5)	1.594(3)
V-O ₅ [L _A]	1.943(5)	2.016(2)	2.020(5)	2.015(3)
V-N [L _A]	2.082(5)	2.039(3)	2.038(6)	2.031(4)
V-O ₆ [L _A]	1.833(4)	1.931(2)	1.920(5)	1.918(3)
V-N v O [L _B]cis	1.861(4)	2.147(2)	2.122(5)	2.148(4)
V-N v O [L _B]trans	2.260(5)	2.360(2)	2.369(6)	2.329(4)

r-5': 5 membered ring V-O-C-N-N; **r-6''**: 6 membered ring V-N-C-C-C-O. L_A denote tridentate Schiff base, L_B

denote co-ligand (maltol, phen or bpy).

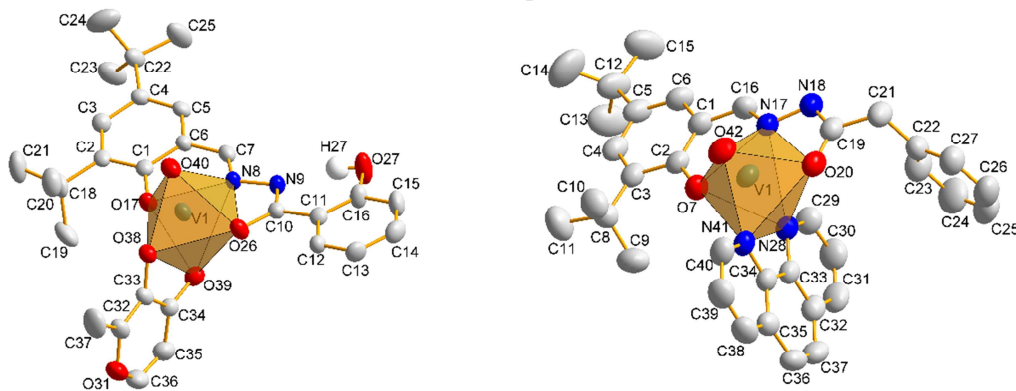


Fig. 1. The molecular structures of complexes **1** (left) and **2** (right) together with the atom labelling scheme. The hydrogen atoms were omitted for clarity. Thermal ellipsoids represent 30% of displacement probability.

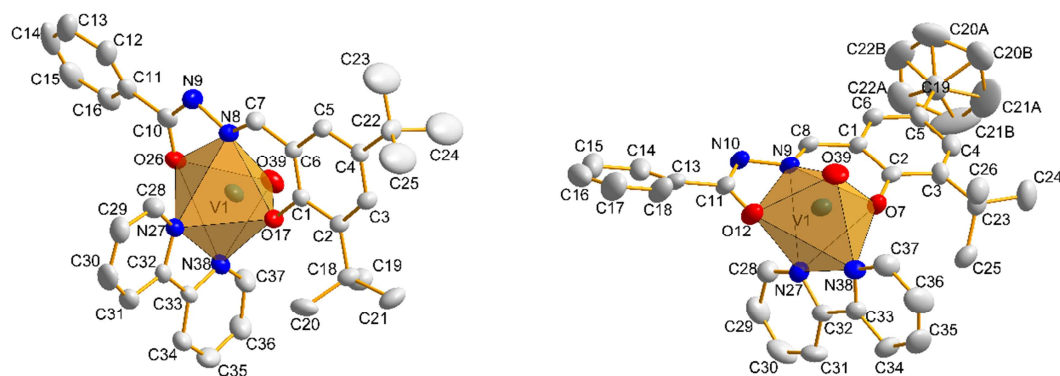


Fig. 2. The molecular structures of complexes **3a** (left) and **3** (right) together with the atom labelling scheme. The hydrogen atoms were omitted for clarity. Thermal ellipsoids represent 30% of displacement probability.

There are two different possibilities of ligand L_A coordination - six membered ring can be on the left side *versus* $V=O$ bond, while 5-membered on the right side, looking from L_B ligand (as in figure shown in Table 2) or in opposite. In the structures of **2**, **3** and **3a** in a single crystal there is a 1 : 1 mixture of both coordination isomers, while in the structure of **1** only a first coordination isomer is present. Both five- and six-membered rings are not lying on the same plane, the highest distortion is observed in deviation of O7 (**2** and **3**) or O17 (**1** and **3a**) of ONO ligand L_A from the plane created on five membered ring. These deviations are: -0.4979 (**1**), -0.4679 (**2**), -0.4085 Å (**3**) and -0.5502 (**3a**) respectively. The highest deviation has complex **3a**, the smallest one - complex **3**. It is unusual, as both complexes have the same coordination sphere. In octahedral square plane, the oxygen (O7 or O17) is present, but also one donating atom (O or N) of L_B ligand. The distortion of square plane is also visible in the deviation of these last atoms from a plane. These deviations are -0.3018 (**1**), -0.5682 (**2**), -0.7763 (**3**) and -0.6389 (**3a**) Å. The distortion of the octahedron is also visible in the bond angles $O=V-L_{trans}$ which are equal to 175.6(2), 166.5(1), 164.2(2) and 164.9(2) ° for **1**, **2**, **3** and **3a** respectively. The $V=O$ bond lengths (Table 2) changes in order **1** < **2** \approx **3** \approx **3a**. The $V-L_{trans}$ bond length should be correlated with the $V=O$ bond through the *trans* effect. Thus the shortest $V=O$ bond should generates the longest $V-L_{trans}$. This is not the case in all studied structures. The shortest $V=O$ bond and $V-L_{trans}$ are in **1**, also such a trend is not observed for the same donating atom in complexes **2-3a** (see Table 2). The *trans* effect can only be driven from the fact that for the same donating atom in L_B ligands bond distances $V=L_{trans}$ are always longer than $V-L_{cis}$ (see Table 2) ones.

The crystal packing for **1-3a** are presented in Figs 3, 4 and 5. The very interesting are the voids calculated for all structures. In **1** and **3** the voids were not found. In **2** the void volume is 727.4 Å³ which is 19.7 % of the total unit cell volume (3692.1 Å³) while in **3a** 1032.6 Å³ with 15.4 % of the total unit cell volume (6692.0 Å³). In the empty places in **3a** the ethanol molecules are probably located, as indicated from elemental analysis, while in **2** the voids are empty. The voids are separated and empty channels in structures of **1**, **2** and **3a** are not observed. For **3** the voids were not found, but as shown in Fig. 5, the channels in structure are observed. The channel diameter is of *ca.* 5 Å and probably methanol molecules is located there. Very interesting is the observation, that small change in synthetic procedure (exchange of methanol into ethanol) results in drastic change in crystal packing and in the anion structure ion **3** and **3a**. Such changes should be caused by the change in strong intermolecular interactions. The observed hydrogen bonds, $\pi \dots \pi$ and C-H $\dots\pi$ interactions in **1-3a** are listed in Tables 3-5 for all studied complexes. In general, in all cases the intermolecular interactions are very weak. For example the relatively short distance O-H-N (intramolecular) in **1** indicates on a very weak interaction due to low angle DHA (152 °). In case of all other hydrogen bonds the distances are much longer and the DHA angles are very low. Thus the hydrogen bonds in all studied complexes are very weak. Thus the most important for packing, for all complexes, are the $\pi \dots \pi$ and C-H $\dots\pi$ interactions listed in Tables 4 and 5 respectively. The interesting is also the illusion, shown in Fig. 3 (left), that the layers are not parallel to each other.

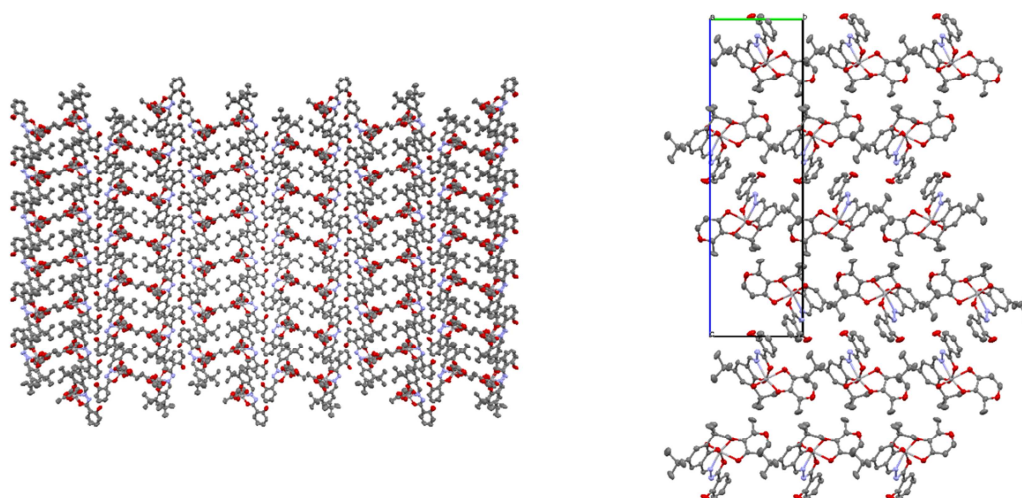


Fig. 3. The crystal packing in **1** through [010] direction (left) and [100] (right). The hydrogen atoms were omitted for clarity. Thermal ellipsoids represent 30% of displacement probability.

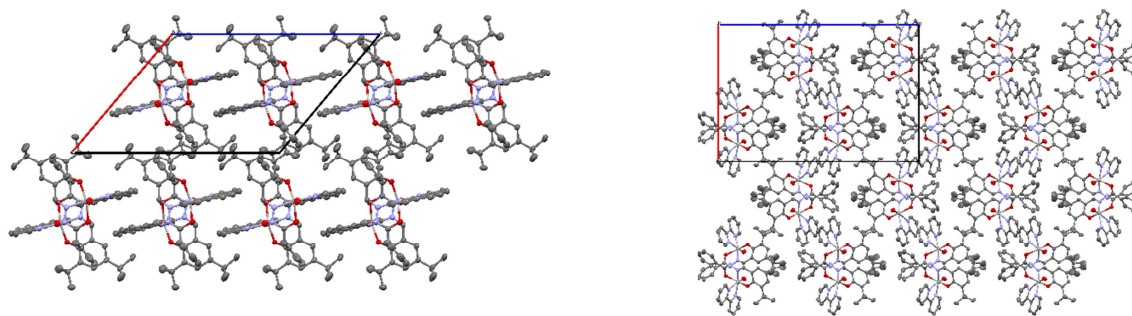


Fig. 4. The crystal packing in **2** (left) and **3a** (right) through [010] direction. The hydrogen atoms were omitted for clarity. Thermal ellipsoids represent 30% of displacement probability.

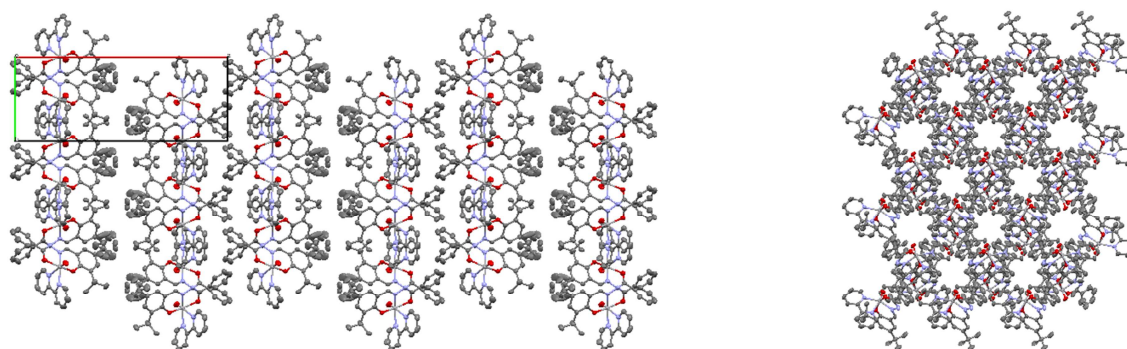


Fig. 5. The crystal packing in **3** through [100] (left) and [010] (right) direction. The hydrogen atoms were omitted for clarity. Thermal ellipsoids represent 30% of displacement probability.

Table 3 Hydrogen bonds for **1-3a** [Å and °].

D-H...A	d(D-H)	d(H...A)	d(D...A)	<(DHA)
1				
O(27)-H(27)...N(9)	0.85(3)	1.85(5)	2.630(8)	152(8)
2				
C(30)-H(30)...O(42) [1-X, -1/2+Y, 3/2-Z]	0.93	2.64	3.484(4)	152.0
C(40)-H(40)...O(42)	0.93	2.57	3.030(4)	110.7
3				
C(34)-H(34)...N(10) [X,1+Y,Z]	0.93	2.47	3.192(9)	134.0
(37)-H(37)...O(39)	0.93	2.50	2.993(9)	113.3
3a				
C(7)-H(7)...O(39) [3/2-X, 1/2+Y,Z]	0.93	2.55	3.387(6)	150.4
C(28)-H(28)...N(8)	0.93	2.66	3.203(6)	118.4
C(34)-H(34)...O(26) [1-X,-Y,1-Z]	0.93	2.54	3.284(5)	137.7
C(37)-H(37)...O(39)	0.93	2.44	2.929(6)	112.9

Table 4 The $\pi \dots \pi$ interactions in **1-3a** [Å].

	$\pi \dots \pi$	shift
1		
Cg(1)...Cg(2) [1+X,Y,Z]	3.963(2)	1.392
Cg(2)...Cg(1) [-1+X,Y,Z]	3.963(2)	1.378
Cg(1): C(1)-C(2)-C(3)-C(4)-C(5)-C(6), Cg(2): C(11)-C(12)-C(13)-C(14)-C(15)-C(16)		
2		
Cg(1)...Cg(4) [1-X,1-Y,1-Z]	3.5935(1)	1.186
Cg(4)...Cg(1) [1-X,1-Y,1-Z]	3.5935(1)	1.234
Cg(4)...Cg(4) [1-X,1-Y,1-Z]	3.9124(1)	1.978
Cg(1): N(41)-C(34)-C(35)-C(38)-C(39)-C(40), Cg(4): C(32)-C(33)-C(34)-C(35)-C(36)-C(37)		
3		
Cg(1)...Cg(2) [1-X,-Y,1-Z]	3.607(3)	1.145
Cg(2)...Cg(1) [1-X,-Y,1-Z]	3.607(3)	1.030
Cg(1): N(27)-C(28)-C(29)-C(30)-C(31)-C(32), Cg(2): N(38)-C(33)-C(34)-C(35)-C(36)-C(37)		
3a		
Cg(1)...Cg(2) [X,1/2-Y,-1/2+Z]	3.692(5)	1.362
Cg(2)...Cg(1)	3.692(5)	1.520
Cg(1): N(27)-C(28)-C(29)-C(30)-C(31)-C(32), Cg(2): N(38)-C(33)-C(34)-C(35)-C(36)-C(37)		

Table 5 The C-H... π interactions in **1-3a** [Å and °].

	H...Cg	X-H...Cg	X...Cg
1			
C(36)-H(36)...Cg(1) [X,1+Y,Z]	2.92	144	3.716(2)
Cg(2): C(1)-C(2)-C(3)-C(4)-C(5)-C(6)			
2			
C(38)-H(38)...Cg(3) [1-X,1-Y,1-Z]	2.70	3.5144(1)	146
C(25)-H(25)...Cg(2) [1-X,1/2+Y,1/2-Z]	2.97	3.7928(1)	148
Cg(2): C(1)-C(2)-C(3)-C(4)-C(5)-C(6), Cg(3): C(22)-C(23)-C(24)-C(25)-C(26)-C(27)			
3			
C(29)-H(29)...Cg(4) [X,-1/2-Y,-1/2+Z]	2.83	156	3.698(11)
C(36)-H(36)...Cg(3) [X,1/2-Y,1/2+Z]	2.63	156	3.501(11)
Cg(3): C(1)-C(2)-C(3)-C(4)-C(5)-C(6), Cg(4): C(13)-C(14)-C(15)-C(16)-C(17)-C(18)			
3a			
C(29)-H(29)...Cg(3) [3/2-X,1/2+Y,Z]	2.89	141	3.656(6)
Cg(3): C(11)-C(12)-C(13)-C(14)-C(15)-C(16)			

IR spectra

The IR spectra of **1 - 3a** are presented in Figs 6 and 7. All complexes have characteristic band located at 969 (for **1**), 953 (for **2**), 957 (for **3**) and 960 cm^{-1} (for **3a**) associated with vibration of V=O group. The position of V=O band is very often correlated with the V=O bond length. The band position can be put in order of decreasing energy as **1** >

$3a \approx 3 > 2$, while the bond length increases in order $1 < 2 \approx 3a < 3$ (see Table 2). As it can be seen, there is no direct correlation between those two trends. But the energy of V=O bond vibration depends also on the strength of the V- L_{trans} bond. As the V=O bond length in **2**, **3a** and **3** is almost equal within experimental error, the V- L_{trans} bond length should be considered. It is changed in order (increasing) $1 < 3a < 2 \approx 3$ as indicated in Table 2. This is in good correlation (within experimental error) with the IR spectra trend indicated above.

The intensive band at ca. 1590 cm^{-1} (1597 (**1**), 1586 (**2**), 1593 (**3** and **3a**)) is attributed to vibration of C=N group in Schiff base ligand and this band was also observed in the other complexes of this type [15,25,26]. Each complex also has bands related to vibrations of co-ligands, for example for **1** the band at 1625 cm^{-1} can be assigned to C=O group in the maltolato ligand. For complex **2** the bands characteristic for 1,10-phenantroline ligand at 1498 , 1424 , 726 cm^{-1} are also observed as well as in the other *d*-electron metal complexes with phen ligand [27]. For complexes **3** and **3a** the spectra are very similar, and only differences in region characteristic for OH vibration of ethanol are observed (see for example at 3300 cm^{-1}) which remains in a good agreement with the structure measurements.

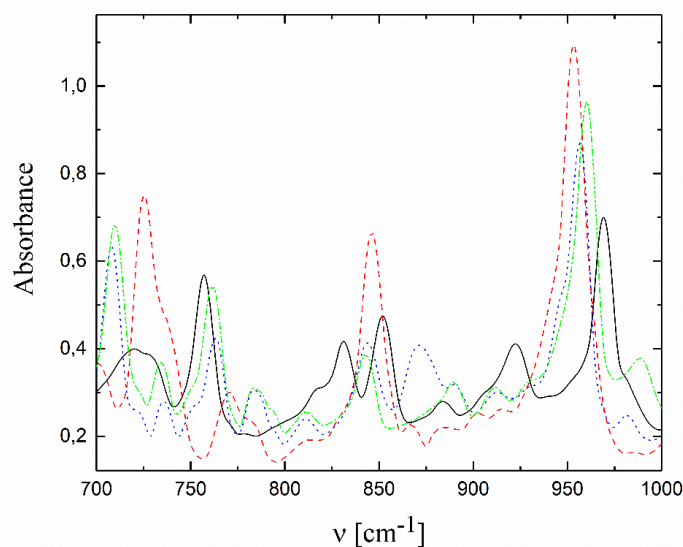


Fig. 6. IR spectra of complexes **1** (black, solid line), **2** (red, dashed line), **3** (blue, dotted line) and **3a** (green, dashed-dotted line) in a $700 - 1000\text{ cm}^{-1}$ range.

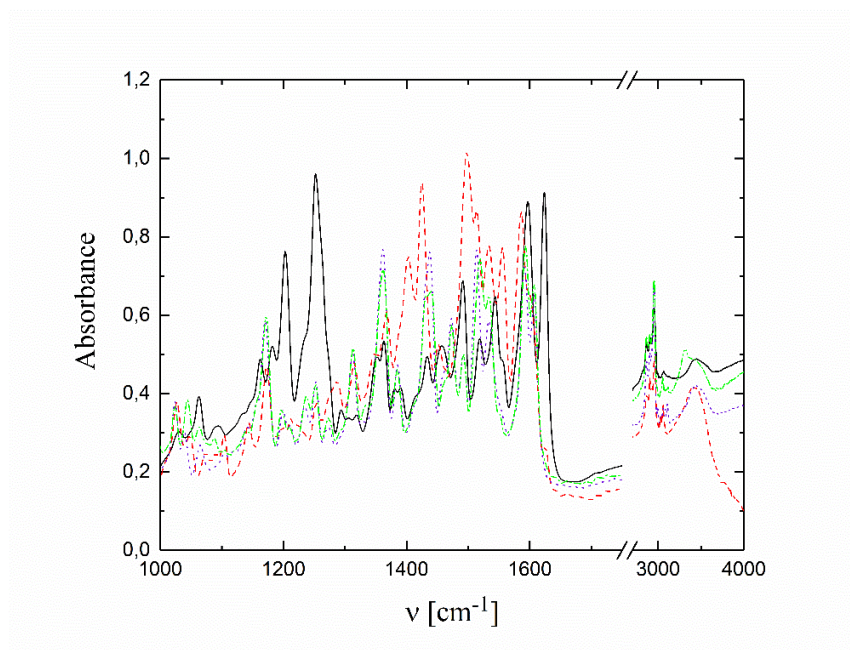


Fig. 7. IR spectra of complexes **1** (black, solid line), **2** (red, dashed line), **3** (blue, dotted line) and **3a** (green, dashed-dotted line) in a 1000 – 4000 cm^{-1} range.

UV-Vis spectra

The selected UV-Vis reflectance spectra of complexes **1** - **3a** are presented in Fig. 8. The reflectance spectra are the most suitable for studying the vanadium oxidation state, as due to low solubility of the complexes studied, *d-d* transitions are invisible in diluted solutions. It can be seen, that in case of **2** and **3a** complexes of V(IV) *d-d* transitions are well observed above 700 nm. For V(V) diamagnetic complexes (**1** and **3** respectively) these bands are not observed. The charge-transfer transitions, connected with the presence of co-ligand, are observed at ca. 550 nm, while those attributed to ONO ligand in the 400-500 nm range. The UV part of the spectra is dominated by the intense bands of co-ligands.

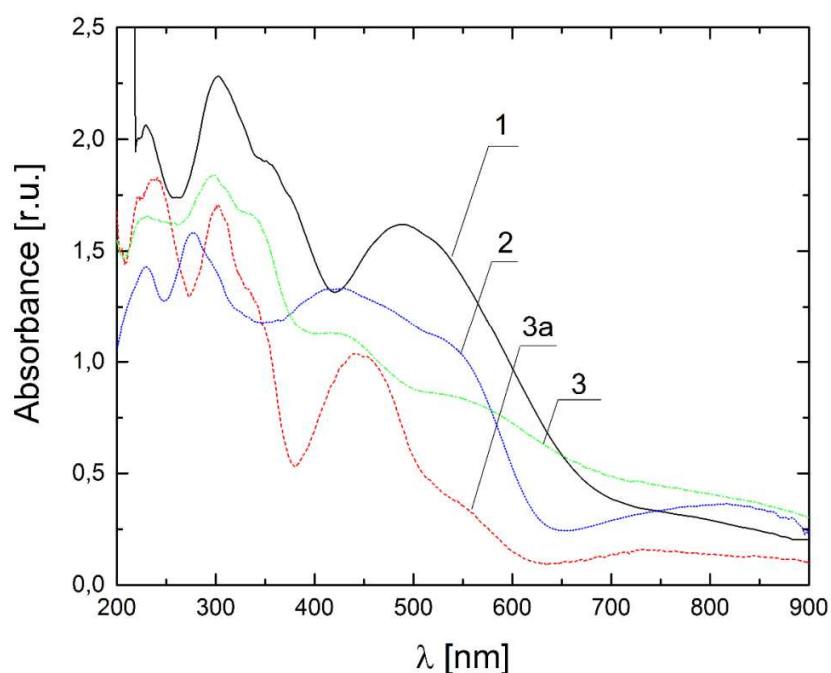


Fig. 8. The UV-Vis reflection spectra of **1** - **3a** after Kubelka-Munk transformations [28]. BaSO₄ as internal white standard.

The selected spectra in solution are presented in Fig. 9. Due to the very high intensity of the bands attributed to ONO ligand, in visible part of the spectra, this band dominates (at ca. 400-500 nm range). As mentioned above, due to low intensity of *d-d* transitions, at concentrations available (due to complex solubility), these bands are not well visible. The molar absorption coefficients in DMSO were estimated for **2** and **3**, as complex **1** was found to be unstable in DMSO. The data are: $\epsilon_{361\text{nm}} = 3.92 \cdot 10^3 \text{ M}^{-1}\text{cm}^{-1}$ and $\epsilon_{324\text{nm}} = 4.67 \cdot 10^3 \text{ M}^{-1}\text{cm}^{-1}$ for **2** and $\epsilon_{510\text{nm}} = 1.55 \cdot 10^2 \text{ M}^{-1}\text{cm}^{-1}$, $\epsilon_{417\text{nm}} = 5.60 \cdot 10^3 \text{ M}^{-1}\text{cm}^{-1}$ and $\epsilon_{330\text{nm}} = 8.40 \cdot 10^3 \text{ M}^{-1}\text{cm}^{-1}$ for **3**. In solution the spectra of **3** and **3a** are essentially the same, as the only difference is the presence of solvent molecule in **3a**. The complexes are solvatochromic, as shown in Fig. 9.

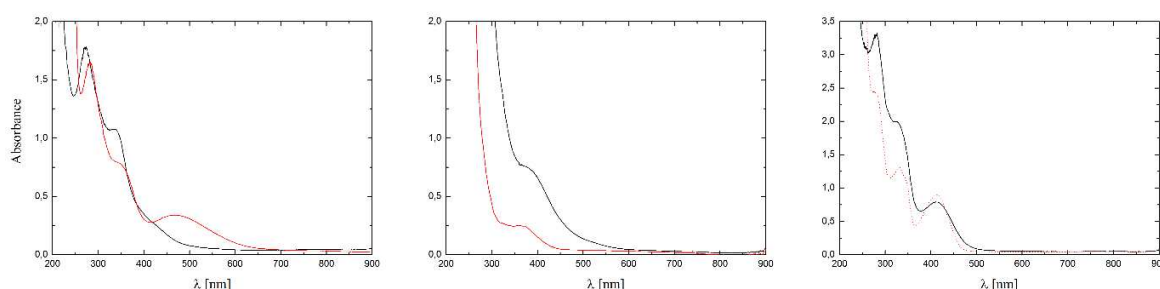


Fig. 9. UV-Vis spectra of **1** (up), **2** (middle) and **3** (down) in EtOH (black line) and DMSO (red line), $d = 1$ cm.

Thermogravimetric analysis

The TG results for complexes **1** and **3a**, measured in air at $10\text{ }^{\circ}\text{C}/\text{min}$, are presented in Fig. 10, while the numerical data are selected in Table 6. The stepwise decomposition of complex **1** is observed. Schiff base ligand decomposes in parts, the mass loss after $372\text{ }^{\circ}\text{C}$ peak indicates that aldehyde is released as first, while hydrazide decomposes later. The decomposition of maltol is a very complicated process, probably involving its oxidation/reduction. Probably part of the oxygen forms vanadium oxides, part of carbon can be a source for carbide formation. These processes are probably responsible for observed constant mass loss, even much above $800\text{ }^{\circ}\text{C}$. For **3a** the decomposition starts at very beginning, but at ca. $270\text{ }^{\circ}\text{C}$ mass loss can be attributed to bpy and EtOH molecule. The almost constant decrease of the mass *versus* temperature is consistent with the X-ray crystal structure determination, when for longer stored crystals only partial occupancy of EtOH molecule was found. For this process, the calculated Δm (32.5 %) fits very well with the observed one (32.2 %). In the next two, a not well resolved processes, ligand L is released. Presence of two separated decomposition processes, at this stage, indicates that the Schiff base ligand L decomposes into components. The first mass loss equal to 34.2 % ($66.4 - 32.2$ %) fits quite well with the release of 3,5-di-tert-butyl-2-hydroxybenzaldehyde (calculated for this process mass loss is equal to 35.1 %) supporting decomposition of ligand L into components (aldehyde and hydrazide) similarly as it was observed for **1**.

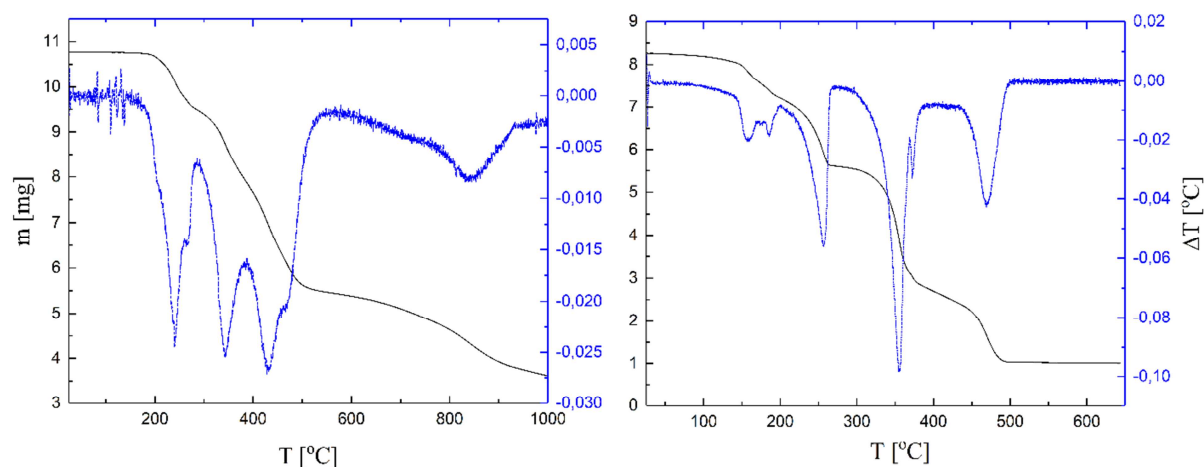


Fig. 10. TG and SDTA curves of **1** (left) and **3a** (right). Scan rate 10°/min, air.

Table 6 Data of thermogravimetric analysis of **1** and **3a**. Scan speed 10°/min, air.

Complex	m [mg]	T _{max} [°C]	Δm _{exp} [%]	Δm _{calc} [%]	Attributed to
1	10.7767				
	9.4659	241			
		268	12.2	11.9	0.18L
	5.4715	343			
		431			
		465sh	49.2	49.3	0.75L
	3.6178	838	66.4	65.9	L
3a	8.26445				
	7.20860	159	12.8	7.41	EtOH
		186			
	5.60710	257	32.2	32.5	EtOH + bpy
	2.78000	356			
		372	66.4	66.6	EtOH + bpy + 0.6L
	1.00440	470	87.8	89.2	EtOH + bpy + L

Cyclic voltammetry

The cyclic voltammetry measurements were performed in DMSO on Pt working and counting electrodes using 0.1M Bu₄NPF₆ as supporting electrolyte and are presented in Figs 11 - 13. The potentials and proper electrochemical processes for **1**, **2** and **3** were summarized in Table 7. As the complexes **3** and **3a** are essentially identical in solution (they differ only by solvent molecule), voltammogram of **3** is presented as representative one for both complexes. For **1** oxidation peaks at +0.050, +0.561 and +0.760 V (at 100 mV/s) are observed. The reduction peaks are at -0.050 and -1.14V. The irreversible processes observed at positive potentials can be attributed to vanadium oxidation

excluding that at +0.050 V. The observed irreversibility of vanadium oxidation (lack of reduction peaks) is artificial one, as oxidation peak show low sensitivity on scan speed change (peak at 741 V shifts to 0.835 V on scan speed change from 20 to 1000 mV/s). This is indicative for reversible processes accompanied by fast chemical changes in oxidized product. The fast decomposition/reduction process makes the reduction peak invisible. This is supported by the data shown in inset in Fig. 11, when longer period the reduction peaks start to be observed (they can be attributed to byproducts formed upon reduction of oxidized forms of vanadium). The peak observed at ca. 0V shows a reversible patterns (see inset in Fig. 11) with the $E_{1/2} = 0.00$ V, with E_a/E_c peak separation of 100 mV and independence of E_a and E_c potentials on scan speed. As such a peak is not visible neither for **2** nor for **3**, it can be attributed to maltolato ligand. The irreversible reduction peak at -1.140 V (at 100 mV/s) can be attributed to ONO ligand. Voltammograms of **2** and **3** can be general interpreted in similar manner. The remarkable difference is observed, however in the negative part of the voltammogram. For **2** the reversible process (see Fig.12) observed at $E_{1/2} = -1.37$ V, with E_a/E_c peak separation of 140 mV, I_a/I_c close to 1.0 and $E_{1/2}$ independent on scan speed, can be attributed to reversible phen ligand redox process. Similar situation was observed earlier for vanadium complexes with phen as ligand, described in literature [15,16]. For complex **3**, reversible peak is observed at -1.388V (E_a , E_c peak separation of 178 mV at 100 mV/s) and can be attributed to bpy reduction (see Fig. 13).

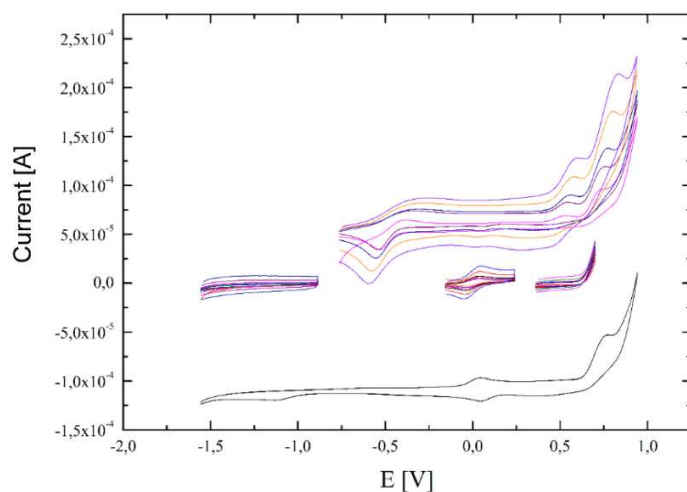


Fig. 11. Cyclic voltammogram of **1** in DMSO. 0.1M Bu₄NPF₆ as electrolyte, Pt working and counting, Ag/AgCl as reference electrodes, potentials *versus* NHE. Scan speeds 100 mV/s (for main curve in full range), insets – scans in selected voltage range, scan speeds in 20 – 1000 mV/s range.

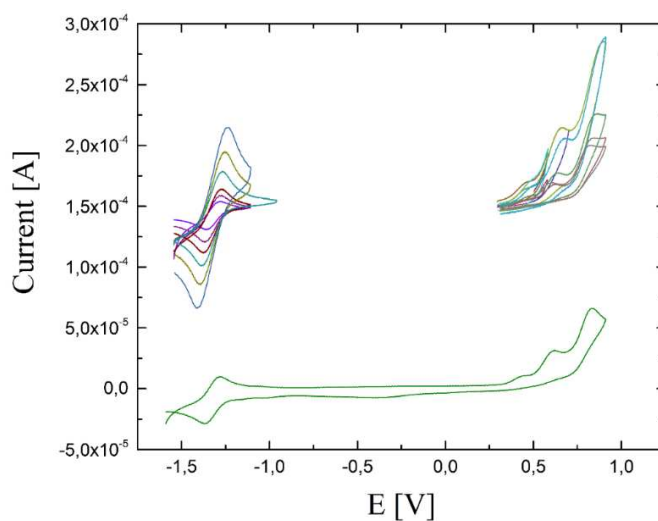


Fig. 12. Cyclic voltammogram of **2** in DMSO. 0.1M Bu₄NPF₆ as electrolyte, Pt working and counting, Ag/AgCl as reference electrodes, potentials *versus* NHE. Scan speeds 100 mV/s (for main curve in full range), insets – scans in selected voltage range, scan speeds in 20 – 1000 mV/s range.

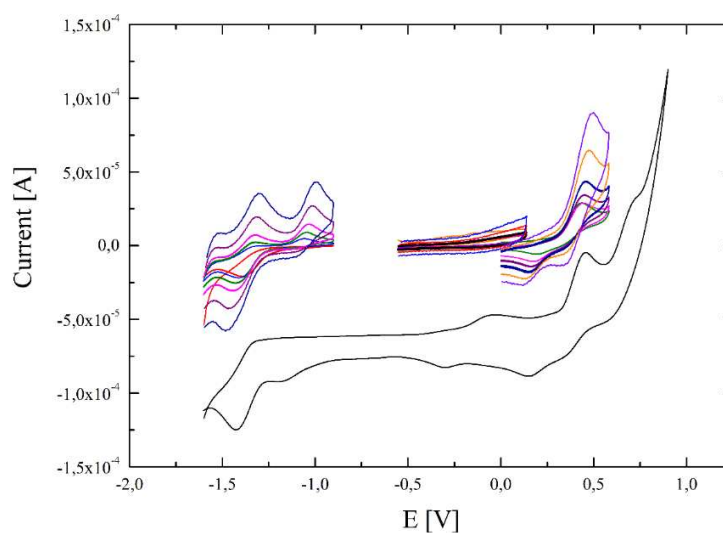


Fig. 13. Cyclic voltammogram of **3** in DMSO. 0.1M Bu₄NPF₆ as electrolyte, Pt working and counting, Ag/AgCl as reference electrodes, potentials *versus* NHE. Scan speeds 100 mV/s (for main curve in full range), insets – scans in selected voltage range, scan speeds in 20 – 1000 mV/s range.

Table 7 Potentials and proper electrochemical processes for **1**, **2** and **3**.

Complex	Potential [V]	Process
1	0.76	$V(IV) - e^- \rightarrow V(V)$
	0.56	$V(III) - e^- \rightarrow V(IV)$
	0.00 ^a	$mal^- - e^- \leftrightarrow mal$
	-1.14	$L_1^{2-} - e^- \rightarrow L_1^-$
2	0.84	$V(IV) - e^- \rightarrow V(V)$
	0.62	$V(III) - e^- \rightarrow V(IV)$
	-1.37	$phen - e^- \leftrightarrow phen^-$
3	0.73	$V(IV) - e^- \rightarrow V(V)$
	0.43	$V(III) - e^- \rightarrow V(IV)$
	-1.39	$bpy - e^- \leftrightarrow bpy^-$

^a E_{1/2}**Stability of complexes in solution**

The stability of complexes in solution plays a crucial role in applications. Fig.14 shows the spectral changes of the solutions of **1** - **3** in DMSO-H₂O mixtures (20 μ L + 3 mL respectively) *versus* time. Again representative data for **3** are presented, similarly as in CV measurements, due to the fact that **3** and **3a** are only outer-sphere solvent molecule isomers. Two different conditions were used – neutral pH (7.00) and pH = 2.00 (pH similar to that in stomach). We used DMSO as a solvent, as all complexes show good solubility in this solvent, mixture was necessary as complexes are almost insoluble in water. DMSO was chosen also due to its applications as a solvent in many pharmaceuticals [29,30]. As indicated in Fig. 14, all complexes are stable in the studied condition, only for **3** a small spectral changes are observed at pH = 2.00. This probably is caused by the flexibility of bpy molecule (in contrary to phen or maltol), which can be stepwise substituted from complex, while both for maltol and phen two bonds have to be broken at the same time. This is supported by the crystal structures of complexes, where stability of complexes cannot be neither driven from distortion observed in coordination sphere (highest for **3** and **3a**) nor from the distance V-L_B (of co-ligand, both for *trans* and *cis* donating atoms of L_B).

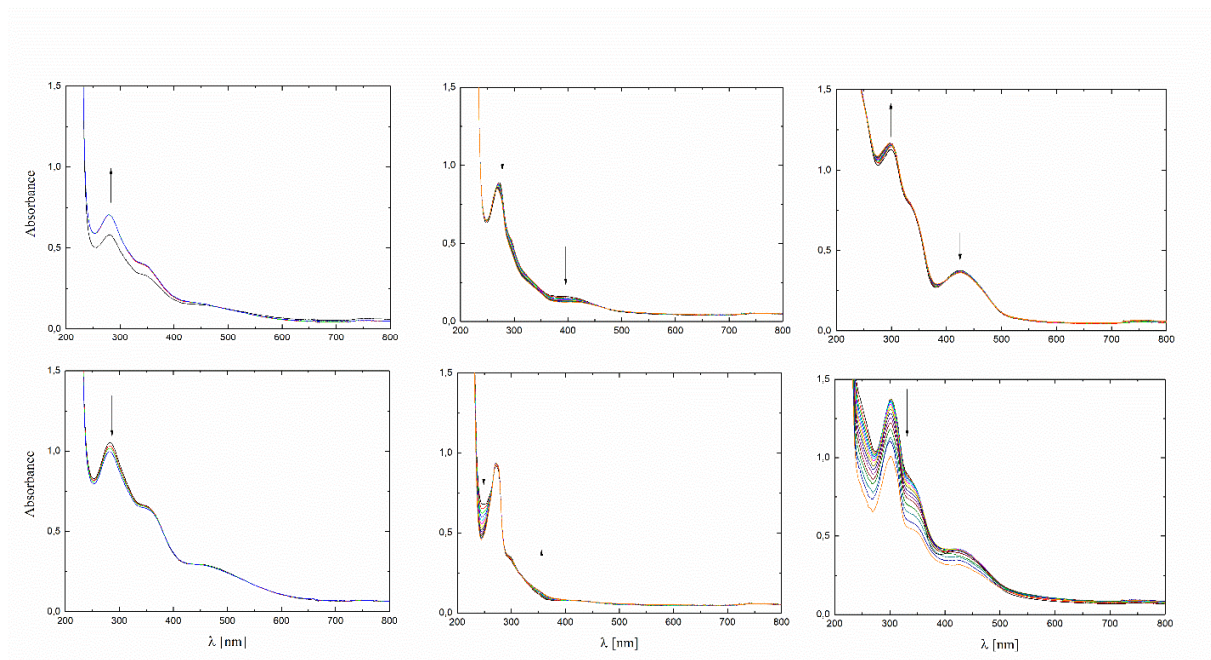


Fig. 14. UV-Vis spectra of **1** (left), **2** (middle) and **3** (right) in DMSO-H₂O (20 μ L + 3 mL) mixture at pH = 7.00 (up) and at pH = 2.00 (down). T = 37 $^{\circ}$ C, spectra measured in 340 s intervals. The arrows indicate the direction of the changes.

Conclusions

Four new complexes of vanadium are described, two of them are the solvation isomers. The X-Ray single crystal structure measurements show a remarkable role of solvent in crystal packing. Small change of methanol into ethanol (in **3** and **3a**) results in dramatic change in packing and symmetry of the crystals. The remarkable role of $\pi \dots \pi$ and C-H $\dots \pi$ interactions on structure is shown, probably as a result of the indicated very weak hydrogen bonds in all studied structures. The *trans* effect was detected for all complexes, elongating the V-L_{trans} (*trans* to short V=O bond) *versus* V-L_{cis} bond distances. In spite of generally very weak intermolecular interactions, in which vanadium donating atoms of ligands do not participate, there is no correlation between V=O and V-L_{trans} distances, even for the same co-ligand as in **3** and **3a**. The V=O band positions in IR spectra were correlated not only with the V=O, but also with the V-L_{trans} distances, while the stability in solution was dependent on the flexibility of the co-ligand ligand. The pharmaceutical activity of investigated complexes, both *in vitro* and *in vivo* studies will be soon presented together with other complexes of similar structure.

Supporting information

CCDC 181172, 1844928, 1850268 and 1848816 of **1**, **2**, **3** and **3a** respectively, contain the supplementary crystallographic data. These data can be obtained free of charge from the Cambridge Crystallographic Data Center via http://www.ccdc.cam.ac.uk/data_request/cif. The cif files of **3a** is included in supplementary materials, together with other experimental data of **1-3a** not included in this paper.

Notes

The authors declare no competing financial interest.

Acknowledgements

This work was partly financed by the European Regional Development Fund under the Innovative Economy Programme 2007–2013 (WND POIG.01.03.01-174/09). The complexes are protected by the patent P.401493.

References

- [1] A.M. Evangelou, Vanadium in cancer treatment, *Crit. Rev. Oncol. Hematol.* 42 (2002) 249-265.
- [2] O.J. D'Cruz, M.U. Fatih, Metvan: a novel oxovanadium (IV) complex with broad spectrum anticancer activity, *Expert Opin. Investig. Drugs* 11 (2002) 1829-1836.
- [3] D.C. Crans, L.N. Yang, A. Haase, X.G. Yang, Health benefits of vanadium and its potential as an anticancer agent, *Met. Ions Life Sci.* 18 (2018) 251-279.
- [4] S.K. Mal, T. Chattopadhyay, A. Fathima, C.S. Purohit, M.S. Kiran, B.U. Nair, R. Ghosh, Synthesis and structural characterization of a vanadium (V)-pyridylbenzimidazole complex: DNA binding and anticancer activity, *Polyhedron* 126 (2017) 23-27.
- [5] P. Jiang, Z. Dong, B. Ma, Z. Ni, H. Duan, X. Li, M. Li, Effect of vanadyl rosiglitazone, a new insulin-mimetic vanadium complexes, on glucose homeostasis of diabetic mice, *Appl. Biochem. Biotechnol.* 180 (2016) 841-851.

- [6] E. Halevas, O. Tsave, M.P. Yavropoulou, A. Hatzidimitriou, J.G. Yovos, V. Psycharis, A. Salifoglou, Design, synthesis and characterization of novel binary V (V)-Schiff base materials linked with insulin-mimetic vanadium-induced differentiation of 3T3-L1 fibroblasts to adipocytes. Structure–function correlations at the molecular level, *J. Inorg. Biochem.* 147 (2015) 99-115.
- [7] C. Carpené, S. Garcia-Vicente, M. Serrano, L. Marti, C. Belles, M. Royo, X. Testar, Insulin-mimetic compound hexakis (benzylammonium) decavanadate is antilipolytic in human fat cells, *World J. Diabetes* 8 (2017) 143-153.
- [8] O. Tsave, S. Petanidis, E. Kioseoglou, M.P. Yavropoulou, J.G. Yovos, D. Anestakis, A. Salifoglou, Role of vanadium in cellular and molecular immunology: association with immune-related inflammation and pharmacotoxicology mechanisms, *Oxid. Med. Cell. Longev.* 2016 (2016) 1-10.
- [9] S. Torabi, M. Mohammadi, M. Shirvani, Antioxidant, antidiabetic, antibacterial and antifungal activities of vanadyl Schiff base complexes, *Trends Pharmaceut. Sci.* 4 (2018) 87-94.
- [10] D. Zamarin, Vanadium: A Panacea for Resistance to Oncolytic Immunotherapy?, *Mol. Ther.* 26 (2018) 9-12.
- [11] M. Selman, C. Rouso, A. Bergeron, H.H. Son, R. Krishnan, N.A. El-Sayes, J.C. Bell, Multi-modal potentiation of oncolytic virotherapy by vanadium compounds, *Mol. Ther.* 26 (2018) 56-69.
- [12] Y. Fu, Q. Wang, X.G. Yang, X.D. Yang, K. Wang, Vanadyl bisacetylacetonate induced G1/S cell cycle arrest via high-intensity ERK phosphorylation in HepG2 cells, *J. Biol. Inorg. Chem.* 13 (2008) 1001-1009.
- [13] I.E. León, N. Butenko, A.L. Di Virgilio, C.I. Muglia, E.J. Baran, I. Cavaco, S.B. Etcheverry, Vanadium and cancer treatment: antitumoral mechanisms of three oxidovanadium (IV) complexes on a human osteosarcoma cell line, *J. Inorg. Biochem.* 134 (2014) 106-117.
- [14] P. Zabierowski, J. Szklarzewicz, R. Gryboś, B. Modryl, W. Nitek, Assemblies of salen-type oxidovanadium(IV) complexes: substituent effects and in vitro protein tyrosine phosphatase inhibition, *Dalton Trans.* 43 (2014) 17044-17053.
- [15] R. Gryboś, J. Szklarzewicz, A. Jurowska, M. Hodorowicz, Properties, structure and stability of V(IV) hydrazide Schiff base ligand complex, *J. Mol. Struct.* 1171 (2018) 880-887.
- [16] R. Gryboś, J. Szklarzewicz, D. Matoga, A. Jurowska, M. Hodorowicz, B. Filipek, J. Sapa, M. Głuch-Lutwin, B. Mordyl, G. Kazek, Vanadium complexes with salicylaldehyde based Schiff base ligands. Variety of coordination modes, oxidation states and pharmaceutical activity, in preparation.

- [17] A. Pasini, M. Gullotti, Schiff base complexes of oxocations part II oxovanadium (IV) complexes with tetradentate optically active schiff bases, *J. Coord. Chem.* 3.4 (1974) 319-332.
- [18] L.J. Hernández-Benítez, P. Jiménez-Cruz, K.E. Cureño-Hernández A. Solano-Peralta, M. Flores-Álamo, A. Flores-Parra, I. Gracia-Mora, S.E. Castillo-Blum, $[V^{IV}O]^{2+}$ complexes: Structure, unusual magnetic properties and cytotoxic effect, *Inorg. Chim Acta* 480 (2018) 197-206.
- [19] G.R. Willsky, A.B. Goldfine, P.J. Kostyniak, J.H. McNeill, L.Q. Yang, H.R. Khan, D.C. Crans, Effect of vanadium (IV) compounds in the treatment of diabetes: in vivo and in vitro studies with vanadyl sulfate and bis (maltolato)oxovanadium (IV), *J. Inorg. Biochem.* 85 (2001) 33-42.
- [20] S. Dümmling, E. Eichhorn, S. Schneider, B. Speiser, M. Würde, Recycling of the Supporting Electrolyte Tetra(n-butyl)ammonium Hexafluorophosphate from Used Electrolyte Solutions, *Current Separations* 5 (1996) 53-56.
- [21] R.W.W. Hooft, COLLECT Nonius BV: Delft, The Netherlands, 1998.
- [22] Z. Otwinowski, W. Minor, *Methods in Enzymology*, Vol. 276, *Macromolecular Crystallography, Part A*, edited by C. W. Carter Jr & R. M. Sweet, New York: Academic Press. 1997, pp. 307–326.
- [23] A. Altomare, M.C. Burla, M. Camalli, G.L. Cascarano, C. Giacovazzo, A. Guagliardi, A.G.G. Moliterni, G. Polidori, R. Spagna, SIR97: a new tool for crystal structure determination and refinement, *J. Appl. Crystallogr.* 32 (1999) 115-119.
- [24] G.M. Sheldrick, SHELXL-2014/7: Program for the Solution of Crystal Structures, University of Göttingen, Göttingen, Germany, 2014.
- [25] N. Raman, Y. Pitchaikani Raja, A. Kulandaisamy, Synthesis and characterisation of Cu(II), Ni(II), Mn(II), Zn(II) and VO(II) Schiff base complexes derived from O-phenylenediamine and acetoacetanilide, *Proc. Indian Acad. Sci. (Chem. Sci.)*, 113 (2001) 183-189.
- [26] G. Asgedom, L. Brammer, L. Kivikoski, R. Valkonen, C.P. Rao. Mononuclear cis-Dioxovanadium(V) Anionic Complexes $[VO_2L]^{-}\{H_2L = 1 + 1\}$ Schiff Base derived from Salicylaldehyde (or Substituted Derivatives) and 2-Amino-2-methylpropan-1-ol: Synthesis, Structure, Spectroscopy, Electrochemistry and Reactivity Studies, *J. Chem. Soc., Dalton Trans.* (1995) 2459-2466.
- [27] A. Schilt, R.C. Taylor, Infra-red spectra of 1: 10-phenanthroline metal complexes in the rock salt region below 2000 cm^{-1} , *J. Inorg. Nucl. Chem.* 9 (1959) 211-221.

- [28] P. Kubelka, F. Munk, Ein Beitrag zur Optik der Farbanstriche, *Z. Tech. Phys. (Leipzig)* 12 (1931) 593–601.
- [29] N.A. Lewis, F. Liu, L. Seymour, A. Magnusen, T.R. Eves, J.F. Arca, F.A. Beckford, R. Venkatraman, A. Gonzalez-Sarrias, F.R. Fronczek, G. VanDerveer, N.P. Seeram, A. Liu, W.L. Jarrett, A.A. Holder, Synthesis, characterisation, and preliminary in vitro studies of vanadium (IV) complexes with a Schiff base and thiosemicarbazones as mixed ligands, *Eur. J. Inorg. Chem.* 4 (2012) 664-677.
- [30] C.P. Kahler, Evaluation of the Use of the Solvent Dimethyl Sulfoxide in Chemiluminescent Studies, *Blood Cells, Molecules, and Diseases* 26 (2000) 626 – 633.

Highlights

- Synthesis and properties of vanadium(IV/V) with Schiff base ligands are described
- Single crystal structures of four complexes are described and discussed
- The X-Ray structure measurements show a notable role of solvent in crystal packing
- The stability in solution in neutral pH and pH = 2.00 is discussed